H 62 10034

NASA TN D-1163

TECHNICAL NOTE

D-1163

INVESTIGATION OF A 10-CENTIMETER-DIAMETER ELECTRON-BOMBARDMENT ION ROCKET

By Paul D. Reader

Lewis Research Center
Cleveland, Ohio

NATIONAL AERONAUTICS AND SPACE ADMINISTRATION

WASHINGTON

January 1962

1W

NATIONAL AERONAUTICS AND SPACE ADMINISTRATION

TECHNICAL NOTE D-1163

INVESTIGATION OF A 10-CENTIMETER-DIAMETER ELECTRON-BOMBARDMENT ION ROCKET

By Paul D. Reader

E-1433

SUMMARY

Previous investigations have proven the feasibility of the electron-bombardment ion source concept. This report deals with an improved 10-centimeter-diameter electron-bombardment ion rocket capable of operation in performance regimes above 10 millipounds of thrust. The source has been operated above 10 millipounds of thrust continuously for 10 hours at a specific impulse of 6500 seconds. The engine was also operated for 150 hours at 4 millipounds of thrust. The source has produced 0.5-ampere beam currents at as low an impulse as 5900 seconds, yielding a calculated thrust of 13 millipounds. Accelerator impingement currents have been on the order of 1 percent of the beam current. Mercury was used as a propellant during this investigation.

INTRODUCTION

Previous investigations have proven the feasibility of the electron-bombardment ion source concept (ref. 1). In determining the performance of a new propulsion device it is a natural tendency to expand the performance envelope as rapidly as possible. The results of the initial investigation using a 10-centimeter source led to the design of a more advanced ion source (ref. 2). The ion rocket which is the subject of this report was fabricated to determine the performance that might be expected from a 10-centimeter-diameter electron-bombardment ion source ion rocket. The second beam source was improved mechanically and simplified electrically, and additional component versatility was provided.

This report deals with the major geometric and electrical parameters affecting the performance of the ion rocket. The ion-chamber geometry was varied by changing such parameters as the ion-chamber length, anode length, and filament position. As part of the ion-chamber investigation, two magnetic-field configurations were also used. The accelerator system was investigated using two different geometries. All electrical parameters were varied over the operational ranges of the ion rocket and

power supplies. The propellant flow rate was also varied. Mercury was used as the propellant throughout the investigation.

SYMBOLS

J current, amp

$\dot{m}$ mass flow, g/sec

P power, w

P_A accelerator power, $(V_I + |V_A|)J_A$

P_B beam power, $V_I J_B$

P_F filament power, $\Delta V_F J_F$

P_I ion-chamber power, $\Delta V_I(J_I - J_B)$

P_M magnet power, $\Delta V_M J_M$

P_T total power, $P_B + P_I + P_M + P_F + P_A$

V potential, v

ΔV potential difference, v

η_P overall power efficiency, P_B/P_T

η_u propellant utilization efficiency, $\dot{m}_B/\dot{m}_T$

Subscripts:

A accelerator

B beam

c calculated

E emission

F filament

I ion chamber

M magnetic field

E-1433

m measured

SD screen distributor

T total

t target

APPARATUS AND PROCEDURE

Engine

The engine is shown in figure 1. A cutaway sketch is included in figure 2. The propellant flows through a calibrated orifice between the boiler and the flow distributor. After leaving the distributor, the flow enters the ion chamber. A field winding surrounding the ion chamber provides a magnetic field roughly parallel to the axis of the ion chamber. Electrons from a hot filament on the axis of the ion chamber bombard the neutrals in the ion chamber, ionizing some of them. The ions of interest pass through the screen which, assuming correct operation, shields the accelerator. The entire engine, with the exception of hot filaments, insulators, the field windings, and one set of accelerator grids, was fabricated of nonmagnetic stainless steel.

Boiler. - Steam at atmospheric pressure was used to heat the double-walled boiler, providing very close thermal control with a minimum of mechanical complexity. The size of the removable calibrated orifice was varied to change propellant flow rates.

Distributor. - The purpose of the distributor is to distribute the flow across the cross section and to shield the high-density flow near the orifice from possible electrical discharges. The distributor used should give an approximately uniform flow distribution across the ion-chamber cross section.

Ionization chamber. - The region between the distributor and the screen is referred to as the ionization chamber. The ionization chamber contains the cylindrical anode and the axial filament. Several chamber lengths and anode lengths are discussed. The filament is a 0.25-millimeter-diameter tantalum wire 2 to 3 centimeters long supported by rods at the axis of the chamber. The filament support rods and anode supports ran through boron nitride insulators, which fitted into tubes running radially outward from the chamber.

Accelerator system. - Two different sets of grids were used as accelerators during this investigation. The first screen and accelerator were constructed of tungsten rods 0.10 centimeter in diameter on

0.51-centimeter lateral centers. The rods were free at the ends so that thermal expansion could take place without causing bowing. When assembled, the axial centerline spacing of the two grids was 0.51 centimeter.

The second set of grids, using 0.48-centimeter axial spacing, was composed of two 0.16-centimeter-thick stainless-steel plates. The plates were drilled with 0.48-centimeter-diameter holes in a hexagonal pattern with 0.64-centimeter center-to-center spacing. The plates were drilled while clamped together to ensure hole alinement.

Field winding. - Enameled copper wire supported on boron nitride blocks was used for the magnetic-field winding. A modified Helmholtz configuration with 64 turns of number 16 wire in each coil was used to give an approximately uniform axial field throughout the ionization chamber. A nonuniform magnetic field was provided by one coil of 120 turns of number 16 wire positioned axially to give the desired degree of field variation throughout the ion chamber. The mean diameter of all the hexagonal shaped coils was 25 centimeters.

Insulators. - Ball insulators were used for all high voltages. All the balls were of fused aluminum oxide about 5 millimeters in diameter (3/16-in. stock size of synthetic sapphire). Some insulators, such as the filament support insulators and the field winding supports, were fabricated of boron nitride. The boron nitride insulators were not subjected to more than 100-volt potential differences.

Assembly of components. - The ionization chamber was bolted directly to the screen grid. The flanges of the screen grid, accelerator grid, and coil mount were fabricated with holes smaller than the insulating balls, so that the balls both positioned and separated the components. Three bolts ran through the assembly to provide the axial compression to keep the balls in place. The flexibility of thin metal sections permitted thermal expansion.

Neutralizer. - A neutralizing filament (20-cm-long, 0.25-mm-diam. tantalum wire) was stretched across the ion beam about 25 centimeters downstream of the engine. A direct current was used to heat the wire (about 100 w), and the negative end was grounded to the vacuum facility. This device was installed primarily to stabilize operation of the ion accelerator. At high beam power levels the wire was moved to the edge of the beam to reduce the erosion due to the ion impingement and prolong the neutralizer filament life.

Electrical system. - A schematic diagram of the electrical system is shown in figure 3.

Facility

The installation of the engine in one of the 5-foot-diameter, 16-foot-long vacuum tanks at the NASA Lewis Research Center is shown in figure 4. The tank has three 32-inch oil diffusion pumps feeding into a common ejector pump, followed by a mechanical pump. With cryogenic pumping used in conjunction with the preceding pumps, engine operation was possible in the 10^{-6}-millimeter-of-mercury pressure range. A more complete description of this facility is included in reference 3.

RESULTS AND DISCUSSION

Experimental results will be discussed in the following order: (1) ion-chamber performance, (2) general characteristics of the accelerator system, (3) ion-chamber - accelerator system interactions, (4) overall engine performance and reliability, and (5) ion-beam thrust and associated target measurements.

Ion-Chamber Performance

A measure of ion-chamber efficiency is the energy dissipated in the ion-chamber discharge per beam ion. In the early configurations where the flow of ionizing electrons was very much greater than the beam current, the power used in the ionization process was regarded as the current collected by the anode times the ion-chamber potential difference. As the beam current, and hence the secondary electron current, became a larger percentage of the current collected by the anode, the ion-chamber loss term was corrected to account for the secondary electrons. The losses are properly written as the ion-chamber potential difference times the difference between the current collected by the anode and the beam current. The power dissipated in the ion-chamber discharge, in electron volts per beam ion, is then arrived at by dividing this dissipated power term by the beam current.

Typical ion-chamber performance for this particular type of electron-bombardment source is shown in the curve of figure 5. The energy dissipated in the ion-chamber discharge is plotted against the ion-chamber potential difference for a constant beam current. As ion-chamber potential difference is lowered, the efficiency of the ion production process increases until a minimum ion-chamber energy is reached at a potential difference of 40 to 50 volts. Below this voltage level large emission currents are required to maintain a given beam current because of the decreasing probability of ionization, that is, cross section (ref. 1). The discharge losses rise and rapidly approach the emission limit of the filament. When a minimum energy is not attained, it is usually due to this emission limit.

Magnetic-field strength. - The effect of magnetic-field strength on ion-chamber performance is shown in figure 6. The energy dissipated in the ion-chamber discharge in electron volts per beam ion is plotted against the magnetic-field strength at the center of the filament. The nonuniform-magnetic-field configuration was used. The ion-chamber potential difference was 50 volts. A 0.125-ampere beam current was maintained at a specific impulse of 7000 seconds. The propellant utilization efficiency was 80 percent. The 1-centimeter anode was positioned at the plane of the center of the filament. The chamber length was 5 centimeters.

The losses drop very rapidly with increasing magnetic-field strength up to about 30 to 35 gauss. After reaching this value the losses tend to level out but still decrease slightly with increasing field strength. The optimum condition is naturally the point at which the sum of chamber losses and magnetic-field losses is minimized.

Magnetic-field shape. - Two magnetic-field shapes were investigated during this program. An approximately uniform field was provided by a Helmholtz coil configuration, modified to give slightly less uniformity but over a greater axial length. The nonuniform field was arranged to give a field at the screen which was 65 percent of the field strength at the distributor when the screen and distributor were approximately 10 centimeters apart. The field strength quoted, in this case, is the field strength 5 centimeters upstream of the screen, the point at which the center of the filament was positioned for the field shape tests. No attempt was made during this investigation to ascertain the optimum magnetic-field configuration.

The effect of the magnetic-field shape on ionization-chamber performance is shown in figure 7. The energy dissipated in the ion-chamber discharge per beam ion is plotted against the ion-chamber potential difference. The upper curve was taken with the uniform magnetic field at a strength of 30 gauss. The lower curve was obtained with a decreasing field in the downstream direction with the 30-gauss strength located at the center of the filament. The beam current was 0.125 ampere and the specific impulse 7000 seconds. The propellant utilization efficiency was again 80 percent. The ion-chamber performance improved when the field strength was decreased in the downstream direction. This trend held for all anode configurations tested during the balance of the investigation.

An explanation of the improved efficiency with the nonuniform magnetic field might be the concentration of high-velocity ionizing electrons at the downstream end of the chamber, so that a greater fraction of the ions produced find their way into the ion beam. Another possible explanation is that the nonuniform magnetic field produces an axial

variation of low-velocity electron density, which, in turn, produces an electric field that tends to direct ions in the downstream direction.

Ion-chamber length. - A considerable portion of the losses incurred in the ion chamber may be due to recombination at the chamber walls, anode, and distributor. Possible performance gains might be expected by reducing the amount of metal surface available to the plasma boundary. To investigate this supposed effect and also to determine possible minimum dimensions of the ion source, the ionization chamber was operated at three lengths: 5, 10, and 17 centimeters. A 1-centimeter-wide anode was used with all three lengths, and the filament was centered at the plane of the anode.

Figure 8 shows the results of these tests. Again, the chamber losses in electron volts per ion are plotted against ion-chamber potential difference for each of the three chamber lengths. The beam current was 0.125 ampere and the impulse 7000 seconds. The propellant utilization efficiency was 80 percent. Figure 8(a) indicates that with the uniform magnetic field the performance improved (lower energy loss per beam ion in the discharge) as the ion chamber was shortened.

The data of figure 8(b), for which the nonuniform magnetic field was used, show the same general improvement as the chamber length was shortened from 17 to 10 centimeters. However, the chamber performance remained substantially the same as the chamber was shortened further. For these tests the 30-gauss field strength was maintained at the center of the filament.

The general trend of results, then, tends to support the theory that the chamber losses increase with chamber area, particularly for the two longest chambers. The lack of improvement in performance for the shortest chamber, especially with the nonuniform magnetic field, indicates that the wall and end areas are not the only significant parameters involved.

Anode length. - Figure 9 shows the effect of reducing the anode length from 15 to 1 centimeter. The discharge loss per beam ion is plotted against the ion-chamber potential difference for a 0.125-ampere beam. The impulse and propellant utilization efficiency are again, respectively, 7000 seconds and 80 percent. In a preliminary report on this electron-bombardment source (ref. 2), it was shown that there was little ion-chamber performance variation for a wide difference in anode length at low beam currents. The results of reference 2 are supported by those of the present investigation at a higher beam current. The two curves of figure 9 show that the performance of the 15- and 1-centimeter anodes is similar with the uniform magnetic field. The two lower curves show that with the nonuniform magnetic field the performance of the chamber with each of the anodes is again very similar. Comparison of

the upper and lower pairs of curves indicates that the beneficial effect of the nonuniform field is slightly greater with the 1-centimeter anode. Similar performance has been obtained with the divergent magnetic field with other anode lengths between 1 and 8 centimeters.

As was shown in the previous section, reducing the wall area reduced ion-chamber losses. Thus, the number of ions recombining on that wall area is probably not negligible. The insensitivity of the ion-chamber losses to anode changes for the same ion-chamber length further indicates that it is unimportant whether this cylindrical wall area is at anode or distributor potential.

In general, the shorter anodes (less than 3 cm) tended to be hard starting in that a higher chamber potential difference has to be used to start the discharge. The discharge was also relatively unstable at low chamber potential differences.

Filament position. - From the data taken during the chamber length tests it was felt that the position of the filament with respect to the divergent field and chamber hardware might have some bearing on the performance of the ion chamber. Figure 10 shows the results of an attempt to determine the effect of axial filament location on the efficiency of the ionization process. The tests were conducted with a 7.5-centimeter-long anode and a 10-centimeter-long chamber. The 3-centimeter-long filament was positioned at the maximum possible upstream or downstream locations. The characteristics were investigated at beam currents of 0.125 and 0.060 ampere. Propellant utilization efficiency was constant at 80 percent and specific impulse at 4500 seconds.

Figure 10(a) shows that the maximum efficiency for both filament positions occurs at an ion-chamber potential difference of 70 volts. The downstream filament gives the best performance at the 0.060-ampere beam current. As mentioned in the general discussion of ion-chamber characteristics, the sharp rise of the dissipated energy below 60 volts for the 0.060-ampere beam is associated with very large emission currents.

Maintaining the same magnetic-field strength in the center of the chamber (5 cm from the screen) and approximately doubling the beam current gave the results shown in figure 10(b). The shape of the two curves is the same, but in this case the upstream filament has superior performance.

It appears, then, that at a beam current of 0.060 ampere a downstream filament location gives better performance, while at a beam current of 0.125 ampere an upstream filament position is superior. It should be pointed out, however, that the difference is, at most, less than 20 percent.

Ion-beam current. - In addition to the effect of filament position, figure 10 also shows the effect of changing the ion-beam current from 0.060 to 0.125 ampere at a specific impulse of 4500 seconds. The effect of this current change was greatest at low ion-chamber potential differences. At 0.060-ampere operation was very inefficient below about 60 volts, while at 0.125 ampere efficient operation could be obtained at the emission limit of the filament at 40 volts. The minimum energy per ion changed less drastically, being about 670 electron volts at 0.060 ampere and 625 electron volts at 0.125 ampere.

Since the performance improved in increasing the ion-beam current from 0.060 to 0.125 ampere, it was of interest to see if a further increase would cause additional improvements. A comparison of ion-chamber performance at 0.125 and 0.25 ampere is shown in figure 11.

The energy dissipated in the ion-chamber discharge per beam ion is plotted against ion-chamber potential difference at a specific impulse of 7000 seconds. The 1-centimeter anode was positioned at the center of the 10-centimeter-long chamber. The propellant utilization efficiency was 80 percent of all beam currents. The 0.125-ampere curve reached a minimum of 380 electron volts per ion at a chamber potential difference of 40 volts. The minimum was not reached at 0.25 ampere because of filament emission limitations. The lowest loss at 0.25 ampere was 530 electron volts per ion. The losses at the higher density condition also increase more rapidly with increasing ion-chamber potential difference.

The decrease in performance (increase in losses) when going from 0.125- to 0.25-ampere beam current has been noted with several other source geometries and appears to be a general phenomenon associated with this size source.

Accelerator Performance

Figure 12 gives a qualitative picture of the beam power distribution for the plate and wire accelerator grid systems. The contours were drawn from data obtained with hot wire and conventional calorimeter traces and with some assistance from observations of impingement patterns at the calorimeter station and projections of patterns on hardware farther downstream. The contours are representative of the power distribution 1 meter from the accelerator system and are given as percents of the maximum value.

As seen in figure 12(a), the power distribution from the plate grids has fairly good radial symmetry. Fifty percent of the beam power is included in a 20° solid angle. The beam current was 0.125 ampere at a specific impulse of 5000 seconds.

The large spread in the power distribution from the wire grids, shown in figure 12(b), is normal to the axis of the grid wires. Fifty percent of the beam power is contained in an elliptical cone estimated to be about 20° by 45°. The beam current was 0.125 ampere at a specific impulse of 6300 seconds.

Figure 13 shows the current density profile across the beam approximately 12 centimeters downstream of the accelerator system. The plot was obtained by recording the impingement current on a 0.475-centimeter-diameter molybdenum disk as it traversed the beam on the horizontal centerline of the engine. The trace was taken using the plate grid accelerator system and operating at 0.125-ampere beam current and a specific impulse of 6000 seconds. The highest current value recorded, at the axis of the source, gave a current density of 37.2 amperes per square meter. The average current density arrived at by dividing the total beam current by the source area is approximately 15 amperes per square meter. The average current density based on the accelerator open area is then about 30 amperes per square meter with a 0.125-ampere beam.

Accelerator impingement currents of less than 1 percent of the beam current could be obtained with both the wire and the drilled plate accelerator systems (fig. 14). The blockage of the wire grids was 37 percent, while that of the plates was 48 percent. The wire grids held the higher voltages (5 to 8 kv) much better than the plate grids. This effect is felt to be due to the sputtering properties of the tungsten wires compared to the stainless-steel plates (8 to 12 percent nickel). Erosion patterns on each set of grids showed that the current density was greatest at the center of the source. The effect of varying accelerating potential is shown in figure 14. The beam current was 0.25 ampere. The propellant utilization efficiency was 80 percent. The nonuniform magnetic field was used, and the ion-chamber potential difference was maintained at approximately 50 volts.

The point where the impingement current rises rapidly with decreasing potential is at the approximate current carrying capacity of the grids. The plate grids, having a slightly shorter acceleration length and perhaps better physical alinement, have better current carrying characteristics at the lower voltages.

Accelerator System - Ion-Chamber Interactions

The relative effects of the various geometry changes investigated are not altered by the impulse level, but the absolute performance level is. Data are available in table I to duplicate, at a lower impulse, most of the figures presented thus far. Figure 15 shows the effect of specific impulse on ion-chamber performance for a 0.25-ampere beam at a propellant utilization efficiency of 80 percent. The ion-chamber

potential difference was 50 volts except for the points below 6000 seconds where it had to be raised to keep from exceeding the emission limit of the filament. The nonuniform magnetic field was used along with the drilled plate accelerator system.

The power dissipated in the ion-chamber discharge per beam ion drops rapidly from a value of nearly 1000 electron volts per ion at a specific impulse of 5000 seconds to a value of 550 electron volts per ion at about 8600 seconds. This effect is probably due to the increased penetration of the accelerator electric field back through the holes in the screen at the large potential differences associated with high impulses.

Overall Engine Performance

The data of table II are indicative of the performance obtainable with this 10-centimeter-diameter electron-bombardment ion rocket. The point with a 0.35-ampere beam at a 6300-second impulse yields a calculated thrust of 10 millipounds. This operating point was held for 10 hours. All the data points except the last five were taken with the stainless-steel plate grids. The last four were taken with the tungsten wire grids. The point at 0.51-ampere beam current at an impulse of 5900 seconds (fifth row from bottom, table II) was taken with molybdenum plate accelerators with 0.24-centimeter-diameter apertures.

The highest efficiency attained during this investigation was 87 percent at a 7750-second impulse. At this impulse and efficiency 206 kilowatts would be required to generate 1 pound of thrust from an array of this type of source.

These data are not presented as representing ultimate or optimum values but only the present state of the art for experimental hardware. Further improvements should certainly be possible in the future. For example, replacing the field coil with a permanent magnet would increase the maximum measured efficiency of 87 to about 89 percent. The efficiency at 5000 seconds would be similarly increased from about 64 to 69 percent.

Endurance Test

To determine the extent of damage to the accelerator during long periods of time, the rocket was operated with a molybdenum accelerator system for 150 hours at a thrust level of 4 millipounds. The beam current was 0.20 ampere at a specific impulse of 5000 seconds. Figure 16(a) shows a general view of the center of the upstream face of the accelerator after the 150-hour run. Figure 16(b) shows a closeup of the

center hole of the accelerator before and after the 150-hour run. The five deep pits surrounding the hole are merely marks to locate the hole.

During the endurance run approximately 230 grams of propellant were accelerated through the grid system. The weight loss of the accelerator was 2.3 grams or about 1 percent of the accelerated propellant mass. No change in plate thickness could be measured with a micrometer. The total time on the accelerator system used for the endurance run was over 200 hours at the conclusion of the run. The useful lifetime of the accelerator system is estimated to be over 1000 hours.

Thrust Target

A 30-centimeter-diameter, 0.5-millimeter-thick stainless-steel disk was mounted on a differential transformer deflection pickup and used as a thrust target during part of the investigation. Thrust measurements were made at comparatively low beam power levels. The maximum target mass was limited by the flexure plates of the pickup to less than 50 grams, thus limiting the size of the disk. Thrust values up to 2 millipounds were observed. Even at these low thrust values the stainless target, located 1 meter from the engine, was heated to incandescence. Previous runs with an aluminum target had resulted in the destruction of the disk.

Because of the weight limitations imposed by the pickup flexure plates, no attempt was made to suppress secondary electrons or trap any sputtered material. The target was isolated electrically so that potential buildup might be measured. Figure 17(a) shows the effect of the neutralizer wire in the beam on the target potential for a range of specific impulse. The maximum potential buildup on the target was +12 volts when the neutralizer was on. When the neutralizer emission was shut off, the potential rose to as much as +1750 volts.

The ion-beam currents intercepted by the target were found by grounding the target through an ammeter. The currents thus obtained are shown in figure 17(b). Because of the deflection of ion trajectories for the floating target potentials measured, the ion-beam current striking the target should be somewhat less than the measured values when the target is isolated electrically and the neutralizer is not used.

The thrust data obtained with the neutralizer on are shown in table III. For the plate accelerator system, the target currents shown in figure 17(b) were used to estimate the percentage of the beam which impinged on the thrust target.

The measured thrust varied from 65 to 96 percent of the estimated value based on beam interception. For the wire grids, the percent of

beam striking the target was estimated from the power distribution profiles of figure 12 to be on the order of 40 to 45 percent. Using the 45-percent rate, the measured thrusts were 71 to 88 percent of the estimated values. If the 40-percent figure is correct, 80 to 98 percent of the estimated thrust was registered by the target.

Since the floating target potential with the neutralizer on was only a few volts, ion trajectories should have been the same whether or not the target was isolated. The momentum effect of sputtered particles should introduce an error, perhaps of the order of 10 percent. The largest errors, however, are probably associated with the estimated percentages of beam interception, which were based on current measurements, both the currents as determined from beam surveys and that from grounding the target. These current measurement errors, which are due to secondary electrons, can easily explain the observed discrepancies between measured and estimated target thrust.

CONCLUSIONS

A nonuniform magnetic field, decreasing in strength in the downstream direction, improves ion-chamber performance. The optimum field strength is approximately 30 gauss at the screen for a 10-centimeter-diameter ion source.

Anode shape is not critical as far as ion-chamber losses are concerned, but shorter chambers (less than 10 cm) perform better than longer chambers. One beneficial effect of a long anode over a short anode for a given chamber length is ease of starting in that a lower potential difference is necessary to start the discharge.

The effect of filament position is significant but depends on ion-beam current.

The minimum ion-chamber discharge losses for the 10-centimeter-diameter ion source occurred at an ion-beam current of 0.125 ampere. The penalties associated with operation at higher or lower ion-beam currents were not large, however, at least for the range investigated from 0.060 to 0.25 ampere.

Accelerator impingement currents of the order of 1 percent of ion-beam current were obtained at impulses from 5000 to 8400 seconds at ion-beam currents up to 0.4 ampere. The life of currently available accelerator systems, estimated from the results of a 150-hour endurance run, should be at least 1000 hours.

Overall power efficiencies of up to 87 percent have been attained with the rocket reported herein.

The thrust measurements made with a thrust target were in substantial agreement with the calculated values from current and voltage measurements.

Lewis Research Center
National Aeronautics and Space Administration
Cleveland, Ohio, September 13, 1961

REFERENCES

1. Kaufman, Harold R.: An Ion Rocket with an Electron-Bombardment Ion Source. NASA TN D-585, 1961.

2. Kaufman, H. R., and Reader, P. D.: Experimental Performance of an Ion Rocket Employing an Electron Bombardment Ion Source. Preprint 1374-60, Am. Rocket Soc., Inc., 1960.

3. Keller, Thomas A.: NASA Electric Rocket Test Facilities. Paper presented at Symposium on Rocket Operations at Simulated High Altitudes and in Space, Arnold Center, Tullahoma (Tenn.), June 28-29, 1961.

TABLE I. - ION-CHAMBER DATA

(a) Effect of magnetic-field strength. Beam current (common ground), J_B, 0.125 ampere; ion-chamber potential difference, ΔV_I, 50 volts; ion-chamber potential, V_I, 4900 volts; accelerator potential, V_A, -1250 volts; propellant utilization efficiency, η_u, 80 percent; chamber length, 5 centimeters; anode length, 1 centimeter; plate accelerators; nonuniform magnetic field

Magnetic-field strength at filament, gauss	Magnetic-field current, J_m, amp	Current collected by anode, J_I, amp	Current collected by accelerator, J_A, amp	Energy dissipated in discharge per beam ion, ev/ion
18.5	4.5	3.20	0.00105	1230
20.5	5.0	2.60	.00082	990
24.6	6.0	1.80	.00083	670
28.7	7.0	1.50	.00082	550
32.8	8.0	1.40	.00086	510
36.9	9.0	1.25	.00085	450
41.0	10.0	1.20	.00087	430
44.1	11.0	1.18	.00083	422
49.2	12.0	1.17	.00085	418
53.3	13.0	1.15	.00090	410
57.4	14.0	1.15	.00087	410
61.5	15.0	1.10	.00088	390
65.6	16.0	1.15	.00090	410
69.7	17.0	1.10	.00095	390
73.8	18.0	1.10	.00090	390
77.9	19.0	1.10	.00090	390
80.0	19.5	1.10	.00090	390

TABLE I. - Continued. ION-CHAMBER DATA

(b) Chamber length and magnetic field shape. Beam current (common ground), J_B, 0.125 ampere; plate accelerators; propellant utilization efficiency, η_u, 80 percent

Magnetic field shape	Ion-chamber potential, V_I, v	Accelerator potential, V_A, v	Magnetic-field potential difference, ΔV_M, v	Magnetic-field current, J_M, amp	Ion-chamber potential difference, ΔV_I, v	Current collected by anode, J_I, amp	Current collected by screen and distributor, J_{SD}, amp	Current collected by accelerator, J_A, amp	Energy dissipated in discharge per beam ion, ev/ion
Chamber length, 5 cm; anode length, 1 cm									
Uniform	2500	-1000	11	7.25	90	2.15	0.74	0.0013	1460
					85	2.13	.68	.0013	1362
					80	2.15	.65	.0012	1295
					75	2.27	.61	.0012	1287
					70	2.25	.54	.0012	1190
					65	2.28	.46	.0011	1120
					60	2.38	.38	↓	1034
					55	2.42	.29		1010
					50	2.52	.17		958
					46	2.70	.10	.0010	389
	4900	-1250	11	7.25	90	1.72	.64	.0015	1147
					85	1.68	.57	.0014	1058
					80	1.68	.51	.0014	976
					75	1.68	.47	.0014	944
					70	1.61	.42	.0013	832
					65	1.70	.38	↓	819
					60	1.73	.34		770
					55	1.80	.28		737
					50	1.80	.19		670
					45	1.95	.10	.0012	657
					40	2.20	0	.0011	664
Non-uniform	2500	-1000	7.5	7.0	90	1.40	----	.0008	918
					80	1.40	↓	↓	817
					70	1.39			708
					60	1.47			645
					55	1.46			583
					50	1.52			558
					45	1.60	↓	↓	531
					40	1.75			520
	4900	-1250	7.5	7.0	90	.95	.15	.00085	675
					85	1.00	.15	.00080	672
					80	1.00	.12	.00085	632
					75	1.00	.10	.00084	593
					70	1.05	----	.00075	556
					65	1.07	↓	-------	516
					60	1.10		-------	478
					55	1.10		.00072	439
					50	1.15		.00070	410
					45	1.30		.00070	423
					40	1.40		.00071	408
					35	1.60	↓	.00071	469
Chamber length, 10 cm; anode length, 1 cm									
Uniform	2500	-1000	11	7.25	90	2.67	0.81	0.0012	1832
					85	2.55	.72	.0011	1651
					80	2.48	.64	↓	1508
					75	2.54	.60		1450
					70	2.50	.53		1330
					65	2.55	.48		1262
					60	2.62	.42		1198
					55	2.65	.34		1111
					50	2.76	.22	↓	1055
	4900	-1250	11	7.25	90	1.85	.62	.0014	1240
					85	1.75	.63	.0014	1105
					80	1.72	.50	.0014	1021
					75	1.80	.48	.0013	1005
					70	1.78	.42	.0012	925
					65	1.85	.38	.0013	898
					60	1.90	.34	.0013	852
					55	1.94	.30	.0012	798
					50	2.10	.25	.0012	790
					45	2.30	.17	.0012	782
					41	2.58	----	------	804
Non-uniform	2500	-1000	6.5	6.0	85	1.24	0.37	0.0002	758
					80	1.28	.37	↓	739
					75	1.28	.36		693
					70	1.28	.35		647
					65	1.35	.34		637
					60	1.37	.33		597
					55	1.43	.32		574
					50	1.51	.30		554
					45	1.66	.28		552
					39	1.86	.22	↓	541
	4900	-1250	7.0	6.0	80	.98	.25	.0002	547
					70	1.02	.24	↓	500
					60	1.05	.23		444
					55	1.12	.22		438
					50	1.15	.20		410
					45	1.22	.19		384
					40	1.30	.16		376
					36	1.62	.07	↓	430

TABLE I. - Continued. ION-CHAMBER DATA

(b) Concluded. Chamber length and magnetic-field shape. Beam current (common ground), J_B, 0.125 ampere; plate accelerators; propellant utilization efficiency, η_u, 80 percent

Magnetic-field shape	Ion-chamber potential, V_j, v	Accelerator potential, V_A, v	Magnetic-field potential difference, ΔV_y, v	Magnetic-field current, J_y, amp	Ion-chamber potential difference, ΔV_T, v	Current collected by anode, J_a, amp	Current collected by screen and distributor, J_{SD}, amp	Current collected by accelerator, J_A, amp	Energy dissipated in discharge per beam ion, ev/ion
Chamber length, 17 cm; anode length, 1 cm									
Uniform	2500	-1000	11	7.25	80	2.70	0.09	0.0020	1310
					75	2.72	.09	.0020	1270
					70	2.75	.09	.0019	1215
					65	2.80	.09	.0019	1240
					60	2.90	.09		1310
					55	3.00	.09		1355
					50	3.10	.09		1405
					45	3.18	.08		1440
					40	3.28	.08		1485
					35	3.41	.08		1542
					30	3.55	.08		1605
	4900	-1250	11	7.25	80	2.60	.07	.0018	1260
					75	2.62	.07		1270
					70	2.65	.07		1285
					65	2.70	.07		1310
					60	2.80	.07		1360
					55	2.90	.07		1405
					50	3.00	.07		1455
					45	3.10	.07		1505
					40	3.20	.07		1555
					35	3.33	.07		1615
Non-uniform	2500	-1000	7.0	6.0	80	1.95	0.03	0.0014	1100
					75	2.00	.02		1120
					70	2.00	.02		1080
					65	2.10	.03		1092
					60	2.15	.03		1117
					55	2.20	.03		1142
					50	2.30	.03	.0013	1170
					45	2.40	.42	.0013	1200
					40	2.50	.42	.0014	1272
	4900	-1250	7.1	6.2	80	1.40	.42	.0013	910
					75	1.50	.43	.0016	925
					70	1.60	.43	.0015	957
					65	1.72	.43	.0015	1776
					60	1.86	.44	.0015	1850
					55	1.70	.40	.0015	1654
					50	1.96	.41	.0015	1791
					45	1.90	.28		1657
					40	2.13	.27		1641
					37	2.72	.22		1980
Chamber length, 17 cm; anode length, 2 cm									
Uniform	4900	-1250	11	7.25	80	1.80	-----	0.0010	1130
					80	1.85			1160
					75	1.92			1075
					70	2.00			1070
					65	2.15			1082
					60	2.30	0.37		1042
					55	2.35	-----		1080
					50	2.50	.30		1080
					45	2.80	-----		1080
Non-uniform	4900	-1250	7.0	6.2	80	1.47	0.24	0.0011	970
					80	1.50	.24		980
					75	1.54	.25		944
					70	1.60	.24		910
					65	1.68	.27		900
					60	1.76	.28		940
					55	1.80	.29		937
					50	1.90	.27		910
					45	1.95	.23		857
					40	2.30	.16	.0012	846
					38	2.40	.15	.0011	891

TABLE I. - Continued. ION-CHAMBER DATA

(c) Filament position. Ion-chamber potential, V_I, 2000 volts; accelerator potential, V_A, -1000 volts; chamber length, 10 centimeters; anode length, 7.5 centimeters; plate accelerators; nonuniform magnetic field; propellant utilization efficiency, η_u, 80 percent

Filament position	Magnetic-field potential difference, ΔV_M, v	Magnetic-field current, J_I, amp	Ion-chamber potential difference, ΔV_I, v	Current collected by anode, J_I, amp	Current collected by screen and distributor, J_{SD}, amp	Current collected by accelerator, J_A, amp	Filament heating potential difference, ΔV_F, v	Filament heating current, J_F, amp	Energy dissipated in discharge per beam ion, ev/ion
Beam current (common ground), J_B, 0.060 amp									
Upstream	8.0	7.0	97	0.62	-0.018	0.0002	---	---	907
			90	.62	-.011				840
			85	.63	-.008				809
			80	.67	.005				813
			75	.68	.010				775
			70	.70	.029				730
			65	.76	.050				759
			60	.82	.083				761
			55	1.22	.185				1080
Down-stream	8.0	7.0	97	0.62	-0.038	0.0002	---	---	907
			90	.60	-.013		5.0	7.2	810
			85	.61	-.007		---	---	778
			80	.59	-.025		---	---	707
			75	.59	-.025		5.0	7.2	662
			72	.62	-.008		---	---	673
			70	.67	.005		---	---	712
			65	.66	.008		---	---	673
			60	.82	.056		5.2	7.8	760
Beam current (common ground), J_B, 0.125 amp									
Upstream	8.0	7.0	97	1.42	0.27	0.0011	5.4	6.1	1005
			90	1.45	.29	.0012	5.4	6.1	956
			80	1.41	.30	.0013	5.5	6.1	823
			70	1.47	.29		5.7	6.2	754
			60	1.55	.28		5.7	6.3	684
			55	1.62	.26		5.8	6.3	656
			50	1.70	.23		6.0	6.3	630
			45	1.88	.19		6.2	6.5	621
			40	2.15	.08	.0014	6.6	6.8	638
	6.5	5.5	97	1.98	.17	.0012	6.0	6.1	1440
			90	1.96	.17		6.0	6.0	1320
			80	1.92	.18		6.1	6.0	1150
			70	1.80	.16		6.0	6.1	939
			65	1.87	.17		6.1	6.2	908
			60	1.87	.17		6.2	6.2	838
			55	1.92	.17		6.2	6.3	790
			50	2.00	.15	.0011	6.3	6.4	750
			45	2.06	.12	.0012	6.4	6.5	697
			39	2.30	.06	.0012	6.7	6.8	678
Down-stream	8.0	7.0	97	1.65	0.22	0.0013	5.3	6.2	1165
			90	1.62	.21		5.3	6.2	1076
			80	1.62	.19		5.3	6.3	987
			70	1.70	.17		5.4	6.3	882
			60	1.70	.15		5.5	6.4	756
			55	1.76	.14		5.6	6.5	715
			50	1.86	.10		5.7	6.6	694
			45	2.05	.01	.0014	---	---	680
			40	2.25	-.76	.0014	6.5	7.2	680
	6.5	5.5	97	2.09	-.12	.0011	5.6	6.2	1523
			90	2.08	-.11		5.7	6.3	1407
			80	2.13	-.08		5.8	6.4	1282
			70	2.18	-.05		5.9	6.5	1101
			65	2.17	-.04		6.0	6.7	1003
			60	2.19	-.02		6.1	6.7	991
			55	2.19	-.02		6.2	6.8	909
			50	2.31	.02		6.4	7.0	876
			48	2.39	.05		6.5	7.0	870

TABLE I. - Concluded. ION-CHAMBER DATA

(d) High beam current and accelerator comparison. Chamber length, 10 centimeters; nonuniform magnetic field; propellant utilization efficiency, η_u, 80 percent

Accelerator type	Beam current (common ground), J_B, amp	Ion-chamber potential, V_I, v	Accelerator potential, V_A, v	Magnetic-field potential difference, ΔV_M, v	Magnetic-field current, J_M, amp	Ion-chamber potential difference, ΔV_I, v	Current collected by anode, J_I, amp	Current collected by screen and distributor, J_{SD}, amp	Current collected by accelerator, J_A, amp	Filament heating potential difference, ΔV_F, v	Filament heating current, J_F, amp	Energy dissipated in discharge per beam ion, ev/ion
Anode length, 1 cm												
Plate	0.250	4500	-1250	7.5	6.0	80	2.70	0.97	0.0032	10.1	6.5	788
						75	2.75	.92	.0032	10.2	6.7	750
						70	2.82	.87	.0032	10.4	6.8	720
						65	2.90	.81	.0031	10.6	7.0	689
						60	2.90	.72	.0031	10.8	7.1	636
						55	3.00	.67	.0031	11.0	7.2	605
						40	3.15	.60	.0030	11.2	7.4	580
						45	3.20	.56	.0030	11.3	7.6	530
	.250	7500	-1250	7.0	6.0	50	3.00	.51	.0031	9.0	15.0	550
		7000					3.10	.57	.0030		15.0	570
		6500					3.22	.56	.0030		15.2	590
		6000					3.25	.57	.0030		15.4	600
		5500					3.25	.58	.0034	8.5	15.6	700
		5000					3.60	.57	.0028	9.0	16.0	670
		4500					3.60	.60	.0027		16.0	700
		4000					3.85	.62	.0028		16.3	720
		3500				53	3.90	.70	.0030			775
		3000				54	4.00	.75	.0035			810
		2750				58	4.00	.78	.0037			825
		2500				60	4.20	.82	.0040			845
		2500				[illegible]	4.37	.98	.0047			857
Anode length, 7.5 cm												
Plate	0.252	6500	-1250	7.5	6.0	50.0	3.05	0.26	0.0020	7.8	10.6	687
	.250	6000	-1500			58.5	3.30	.48		7.4	10.8	734
	.260	5600	-1000			59.0	3.25	.44		7.4	10.3	677
	.255	5300	-1100			58.5	3.29	.45		7.4	10.2	693
	.250	4000	-1250			58.0	4.30	----	.0030	7.6	11.0	940
Wire	0.250	6250	-1700	7.0	6.3	50.0	2.30	0.23	0.0022	7.1	10.4	410
		6000	-1500				2.15	.20	.0022	6.3	10.5	3 9
		5500					2.40	.21	.0025	7.1	10.7	430
		5000					2.55	.21	.0030	7.2	10.[illegible]	460

TABLE II. - OVERALL ENGINE PERFORMANCE

[Nonuniform magnetic field.]

Ion-chamber potential, V_-, v	Accelerator potential, V_A, v	Beam current (common ground), J_B, amp	Magnetic-field potential difference, ΔV_M, v	Magnetic-field current, J_M, amp	Ion-chamber potential difference, ΔV_I, v	Current collected by anode, J_I, amp	Current collected by accelerator, J_A, amp	Filament heating potential difference, ΔV_F,	Filament heating current, J_F,	Energy dissipated in discharge per beam ion, ev/ion	Specific impulse, sec	Overall power efficiency, η_P, P_B/P_T	Thrust, mlb
4000	1100	0.250	7.0	6.5	55	3.35	0.0025	[illegible]	10.0	682	8300	0.772	7.2
7000	1400	.250	↓	6.1	50	3.10	.0020	7.3	10.2	570	8400	.763	8.4
4800	1250	.250	↓	6.0	45	3.20	.0030	7.6	11.3	831	8300	.811	7.9
2500	1000	.125	6.0	↓	50	1.51	.0002	6.7	10.8	584	8000	.837	2.9
2500	1000	.125	6.0	↓	55	1.43	.0002	6.8	10.7	574	8000	.836	2.9
5500	1250	.340	7.0	↓	62	4.30	.0040	7.6	11.0	722	7400	.824	11.4
5800	1250	.405	↓	↓	74	4.30	.0040	7.6	11.0	803	7600	.831	14.0
6500	1250	.400	↓	↓	68	5.00	.0042	8.4	11.0	782	8050	.844	14.8
4000	1400	.350	9.0	6.5	55	5.00	.0050	10.0	20.0	731	6300	.721	10.0
3500	500	.810	7.0	5.6	47	8.40	.0065	9.0	22.0	727	5900	.738	13.8
6250	1750	.250	↓	6.3	50	2.30	.0022	7.1	10.4	410	7300	.867	8.0
6000	1500	.250	↓	↓	↓	2.15	.0022	6.9	10.5	380	7750	.886	8.8
5500	1500	.250	↓	↓	↓	2.40	.0025	7.1	10.7	430	7400	.848	8.4
5000	1500	.250	↓	↓	↓	2.55	.0050	7.2	10.9	460	7070	.822	8.2

TABLE III. - THRUST TARGET DATA

(a) Thrust measurements

Accelerator system	Specific impulse, sec	Beam current (common ground), J_B, amp	Target current, J_t, amp	J_t/J_B	Theoretical thrust, F_c, mlb	Estimated target force, $J_t/J_B \times F_c$, mlb	Measured thrust, F_m, mlb	Measured thrust/ Estimated target force
Plate	5000	0.125	0.037	0.296	2.87	0.85	0.55	0.65
↓	5000	.125	.037	.296	2.87	.85	.62	.73
	6300	.127	.070	.550	3.63	2.00	1.93	.96
	5500	.127	.050	.395	3.08	1.21	1.10	.91
Wire	6300	.126	-----	.40	3.63	1.45	1.43	.98
				.45	3.63	1.63	1.43	.88
Wire	6300	.200	-----	.40	5.82	2.33	1.87	.80
				.45	5.82	2.62	1.87	.71

(b) Thrust target voltage and current. Beam current (common ground), J_B, 0.125 ampere; accelerator potential, V_A, -1250 volts; chamber length, 10 centimeters; anode length, 7.5 centimeters; plate accelerators; nonuniform magnetic field

Heated filament neutralizer	Target potential, V_T, v	Current collected by target, J_T, amp	Ion-chamber potential, V_I, v	Magnetic-field potential difference, ΔV_M, v	Magnetic-field current, J_M, amp	Ion-chamber potential difference, ΔV_I, v	Current collected by anode, J_I, amp	Current collected by screen and distributor, J_{SD}, amp	Current collected by accelerator, J_A, amp
Off	770	0.025	2000	7.0	6.3	60	1.53	0.11	0.0013
	1010	.038	2500	↓	6.0	65	1.45	.11	.0012
	1280	.049	3000		6.4	48	1.38	.09	.0011
	1550	.061	3500		6.4	46	1.35	.08	.0010
	1750	.072	4000		6.35	44	1.32	.07	.0011
On	10	0.026	2000	7.0	6.3	60	1.53	0.11	0.0013
	11	.039	2500	↓	6.0	65	1.45	.11	.0013
	11	.050	3000		6.4	48	1.38	.09	.0011
	12	.063	3500		6.4	46	1.35	.08	.0010
	12	.073	4000		6.35	44	1.32	.07	.0011

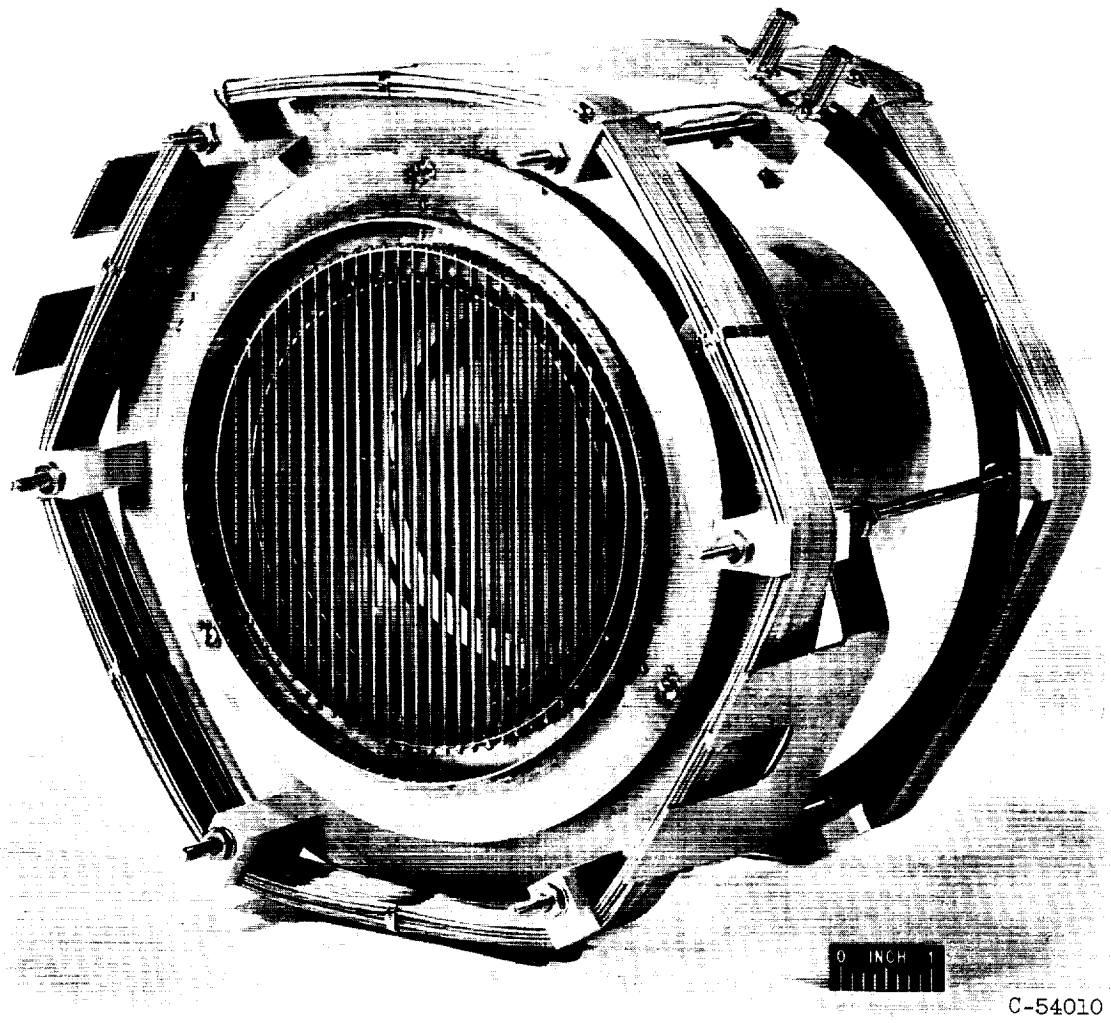

Figure 1. - Electron-bombardment ion engine.

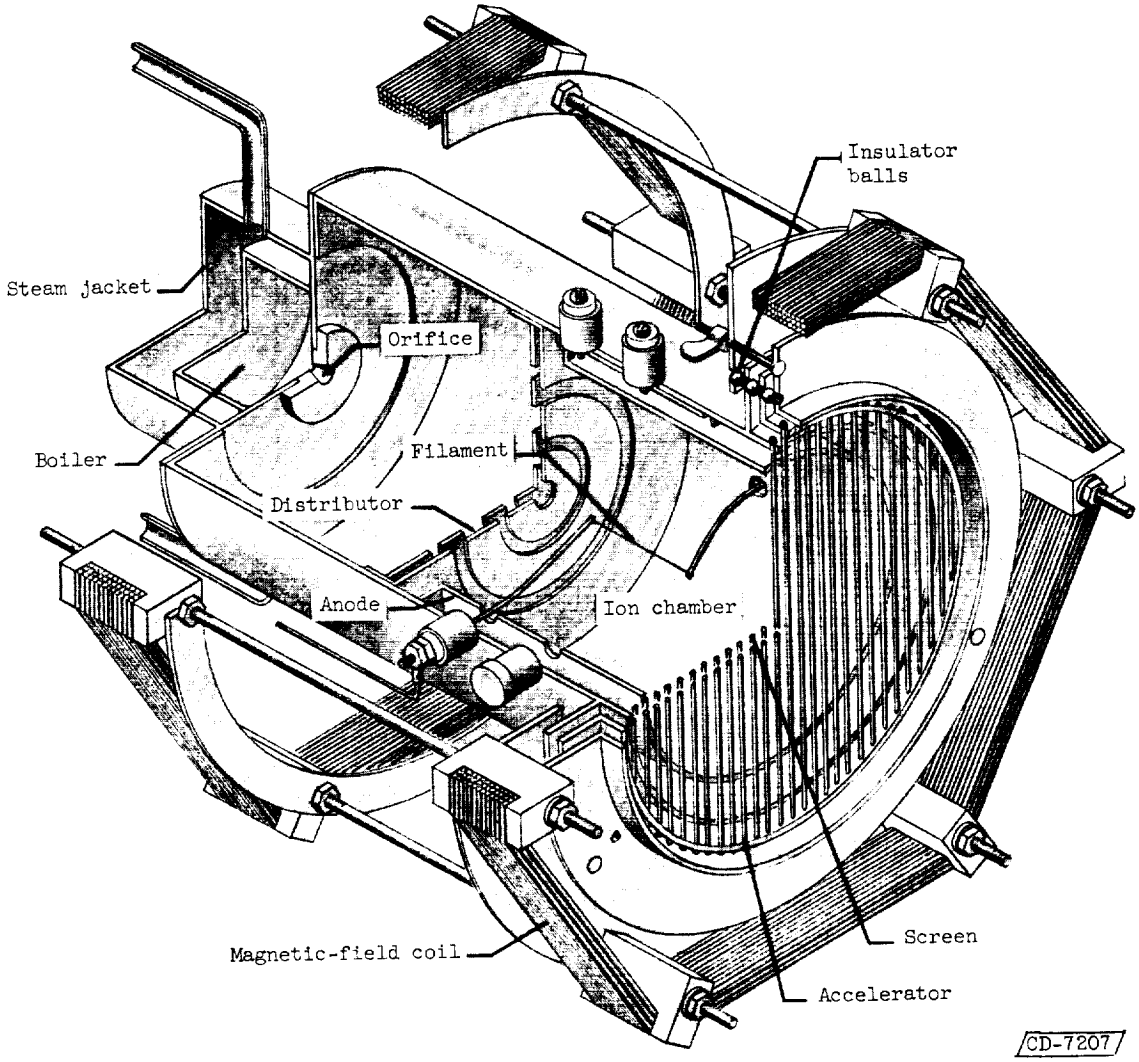

Figure 2. - Cutaway sketch of engine.

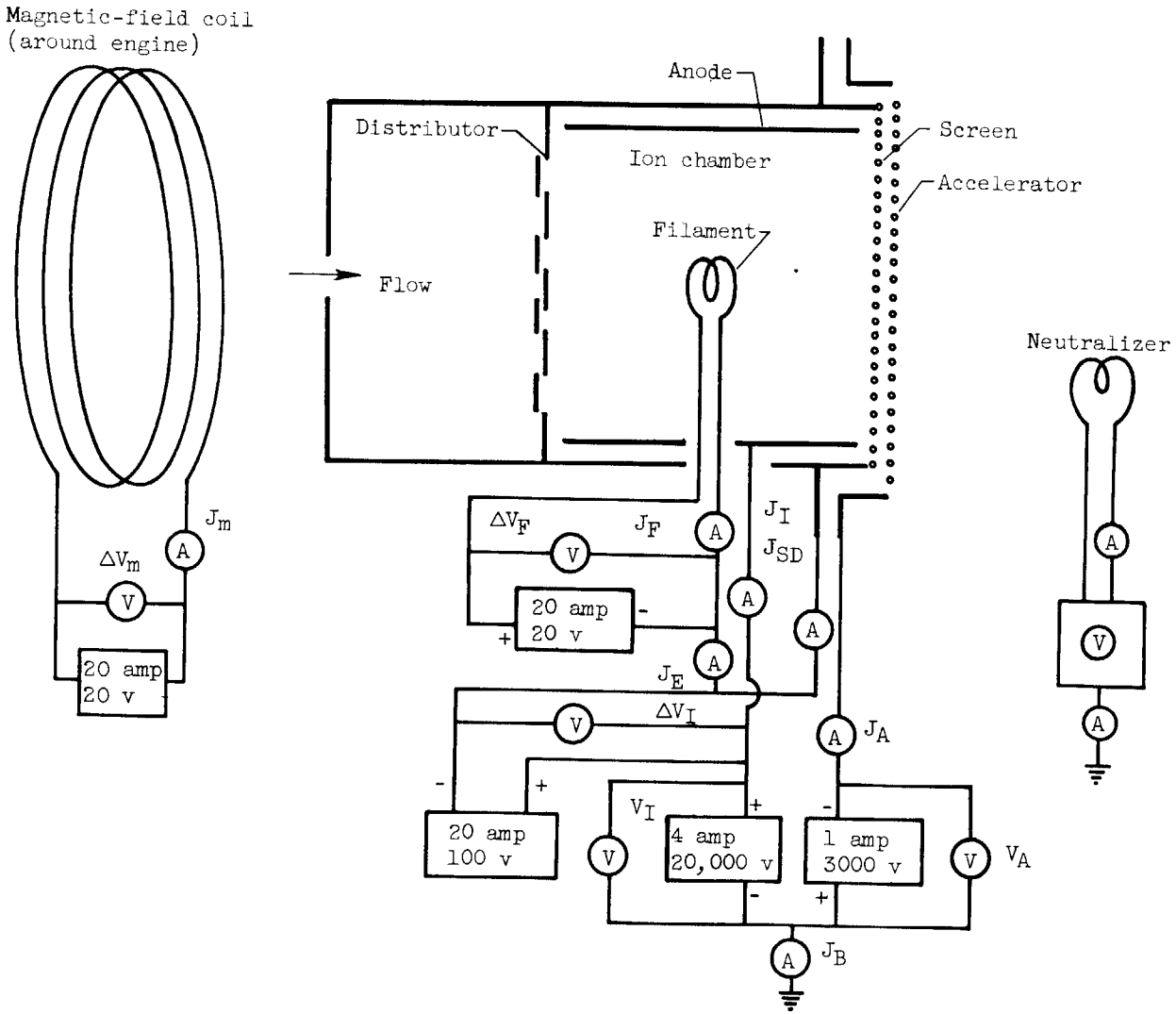

Figure 3. - Wiring diagram of ion engine.

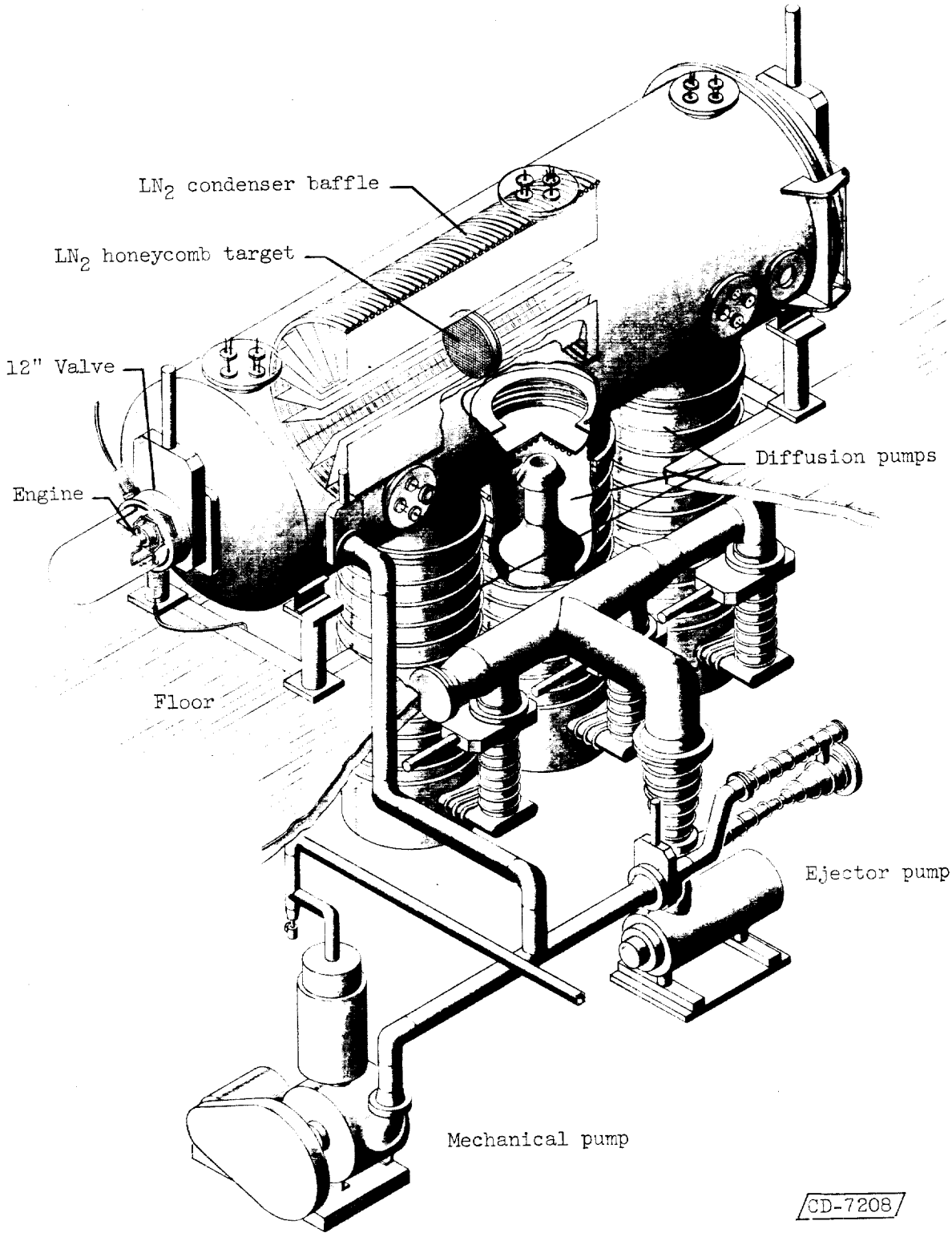

Figure 4. - Sketch of complete engine and vacuum-tank installation.

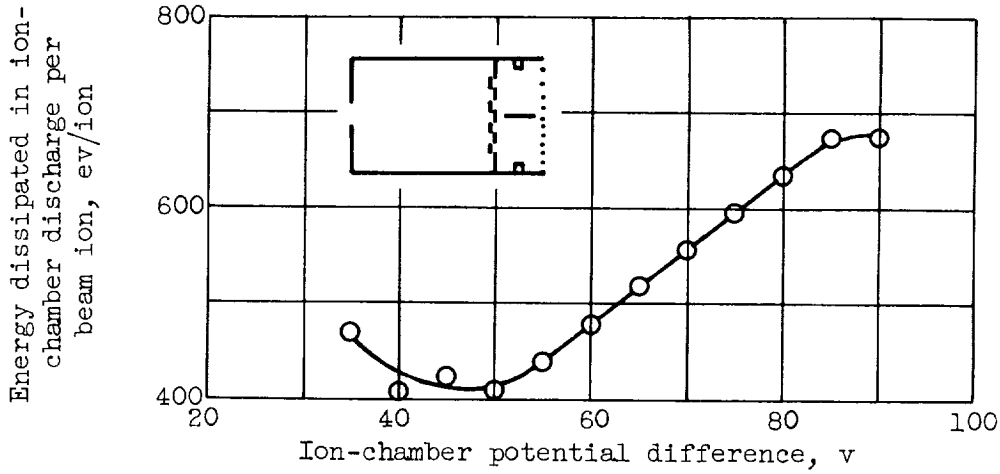

Figure 5. - General ion-chamber performance characteristics. 0.125-Ampere beam current at a specific impulse of 7000 seconds; nonuniform magnetic field with strength of 32 gauss at center of filament; propellant utilization efficiency, 0.75.

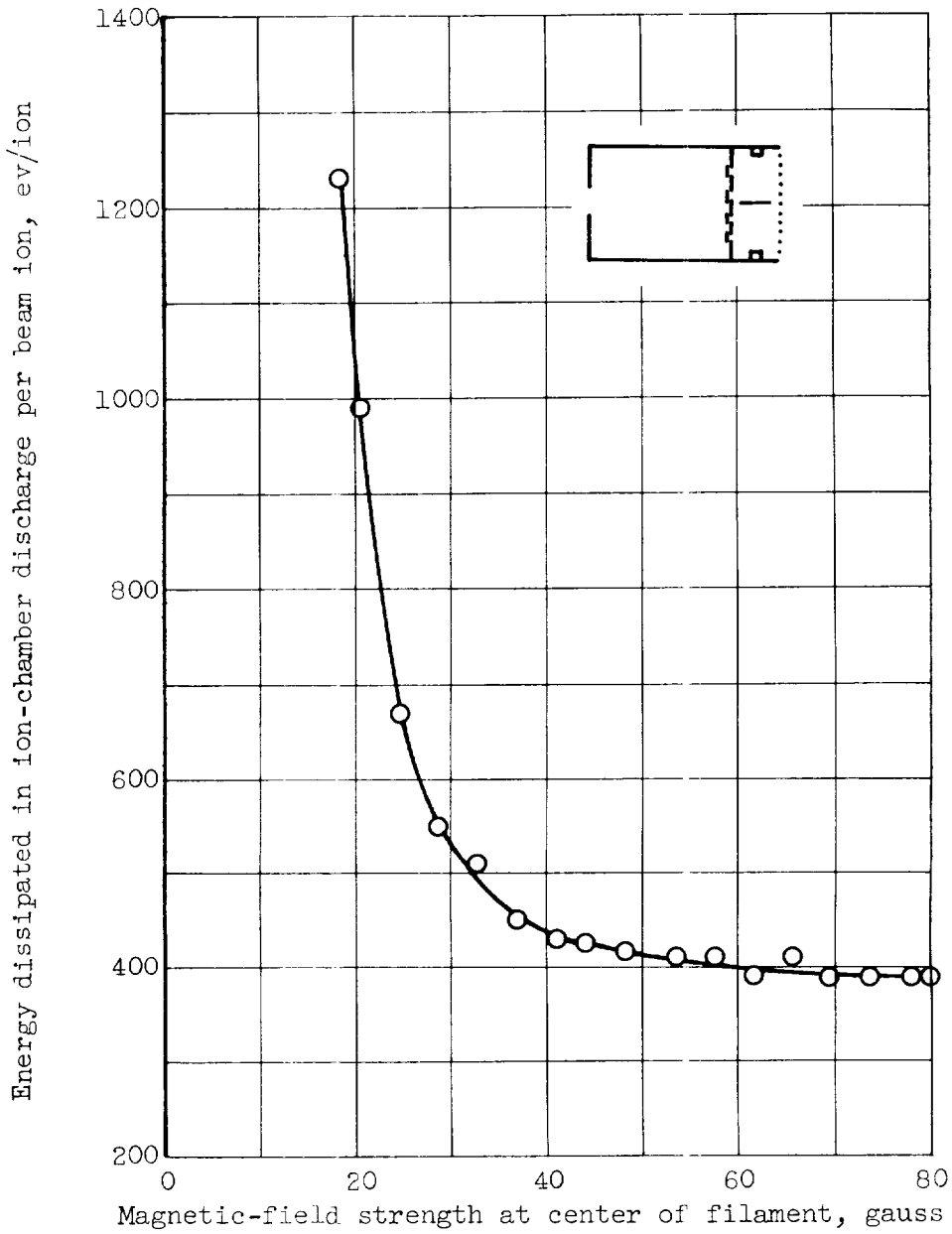

Figure 6. - Effect of magnetic-field strength on ion-chamber performance. 0.125-Ampere beam current at a specific impulse of 7000 seconds; ion-chamber potential difference, 50 volts; propellant utilization efficiency, 0.8.

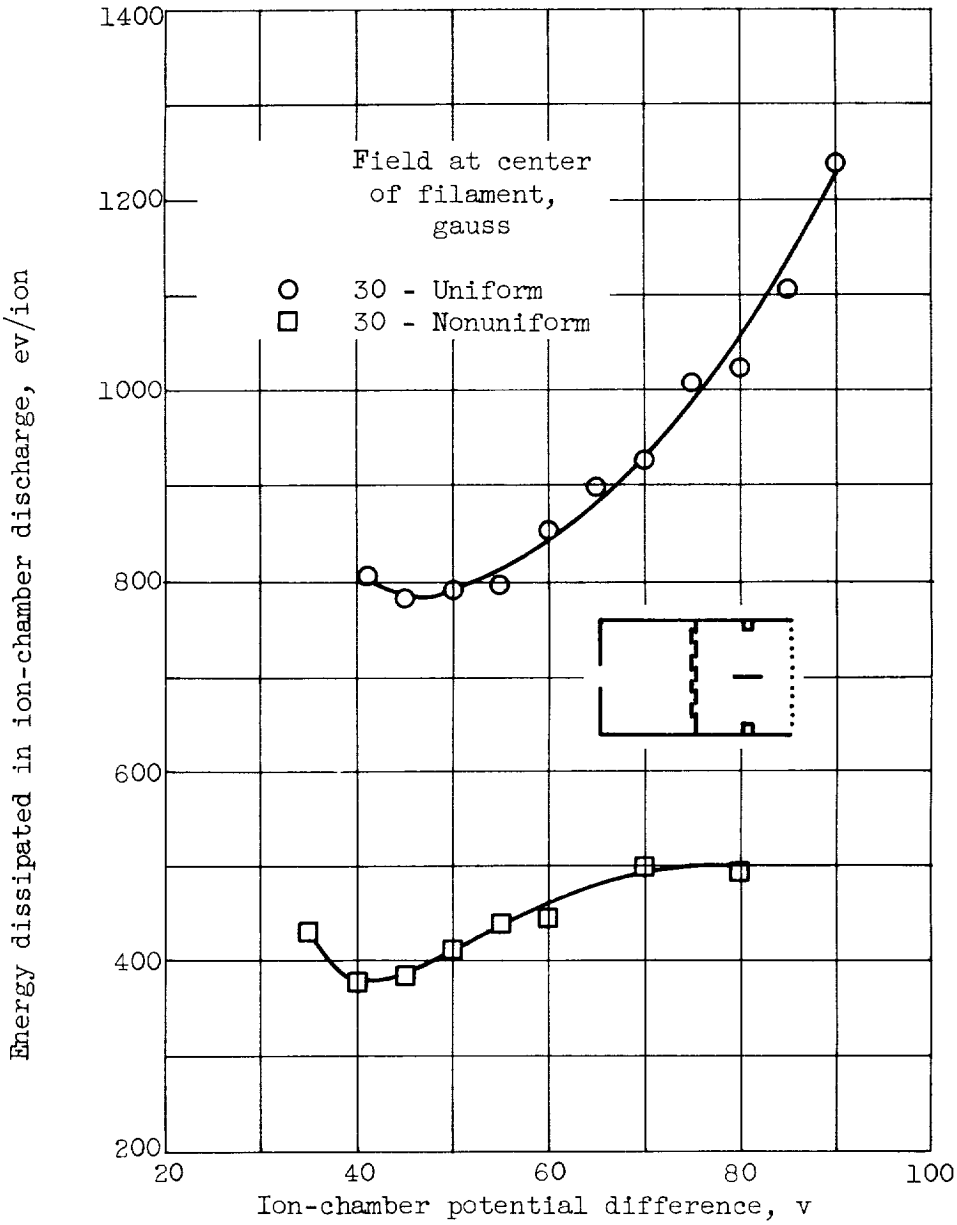

Figure 7. - Effect of magnetic-field shape on ion-chamber performance at a beam current of 0.125 ampere. Specific impulse, 7000 seconds; 1-centimeter anode was used with a 10-centimeter chamber length.

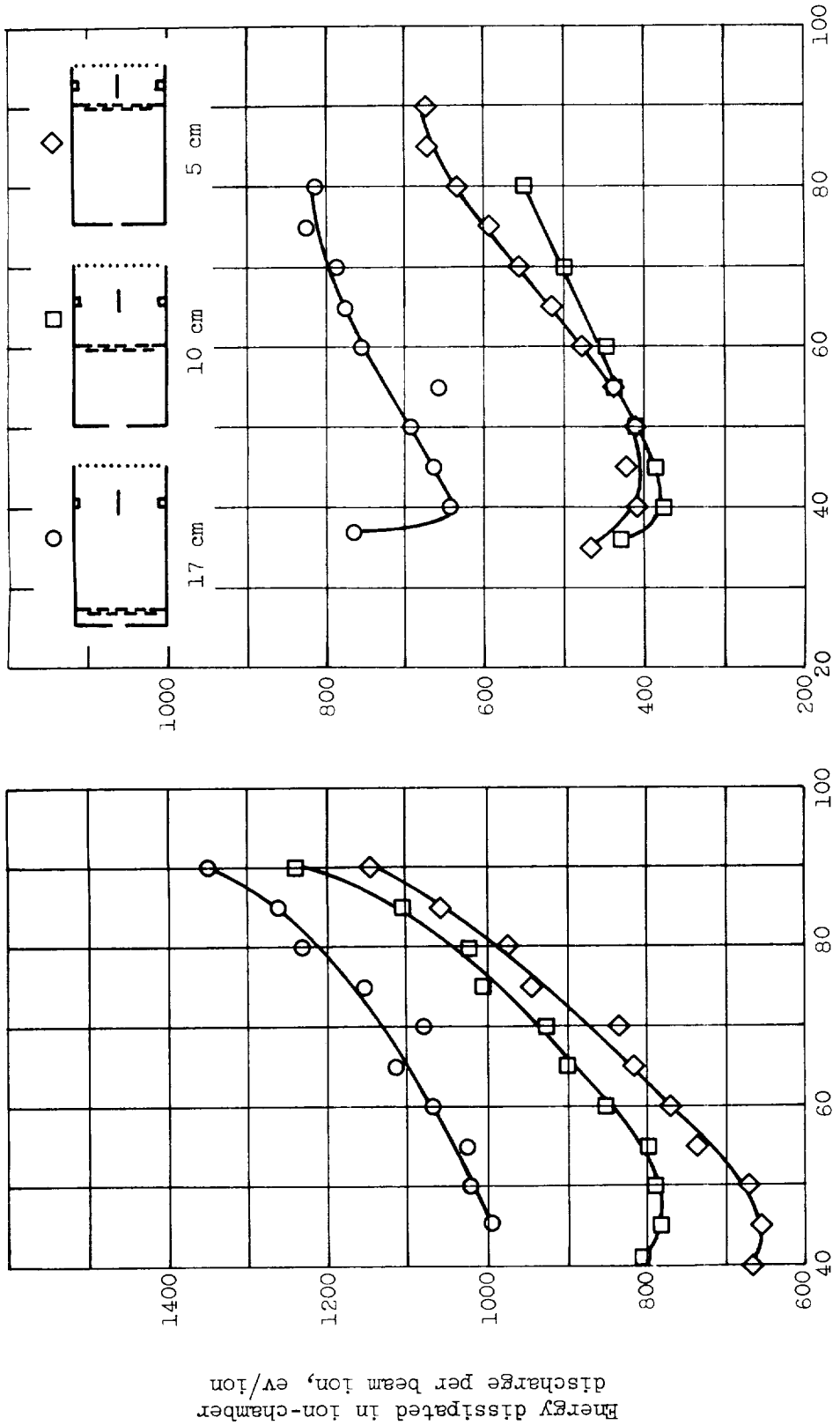

(a) Uniform magnetic field, 30 gauss at filament.

(b) Nonuniform field, 30 gauss at filament.

Figure 8. - Effect of chamber length on ion-chamber performance. 0.125-Ampere beam current at specific impulse of 7000 seconds.

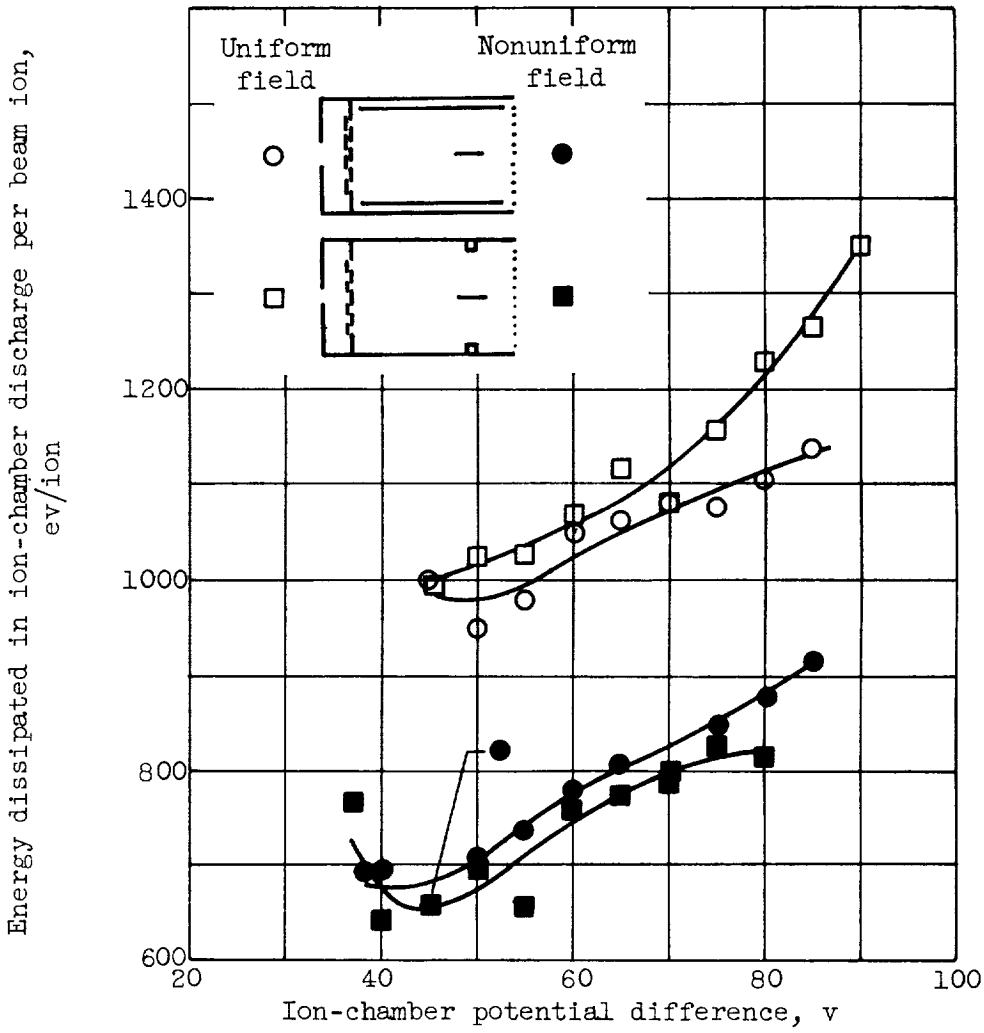

Figure 9. - Effect of anode length on ion-chamber performance with 30-gauss field strength at the filament. 0.125-Ampere beam current at 7000-second impulse; ion-chamber length, 17 centimeters.

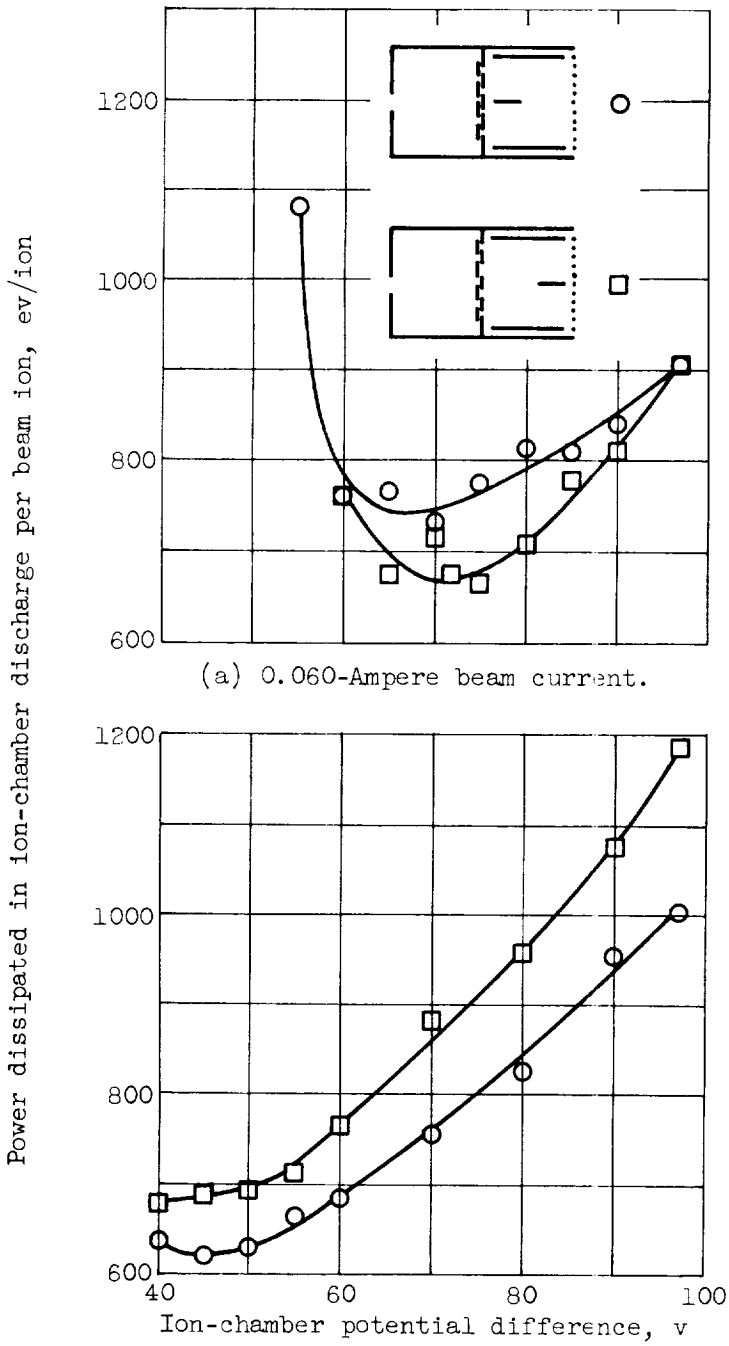

Figure 10. - Effect of filament position on ion-chamber efficiency. Nonuniform magnetic field with strength of 35 gauss at center of chamber; specific impulse, 4500 seconds; a 7.5-centimeter-long anode was used in a 10-centimeter-long ion chamber.

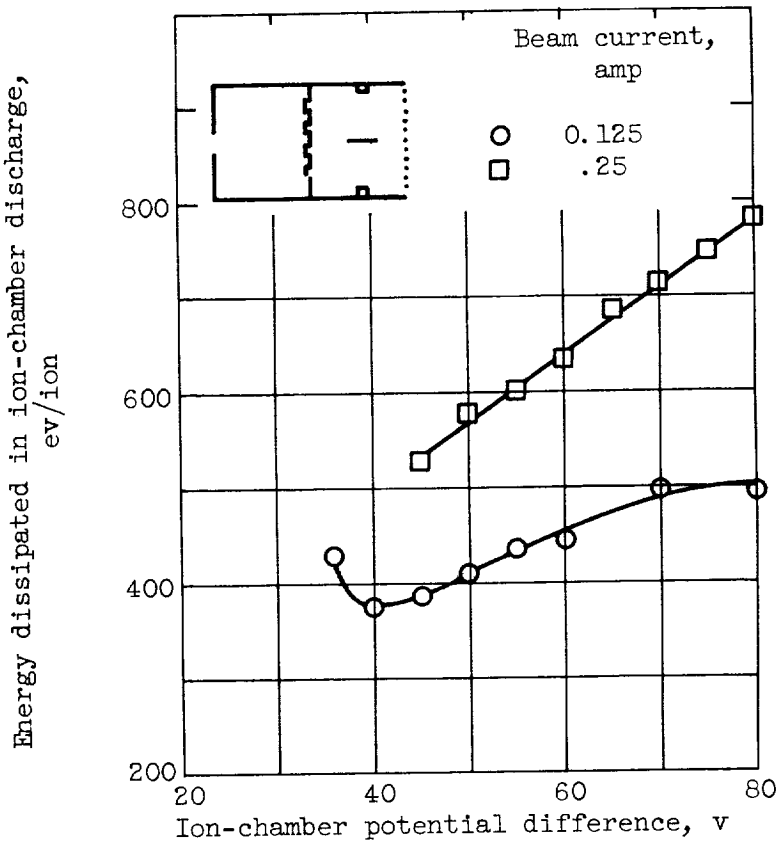

Figure 11. - Effect of beam current on ion-chamber performance at a specific impulse of 7000 seconds. Nonuniform magnetic-field strength, 30 gauss at center of chamber; propellant utilization efficiency, 80 percent; 1-centimeter-long anode used in 10-centimeter-long ion chamber.

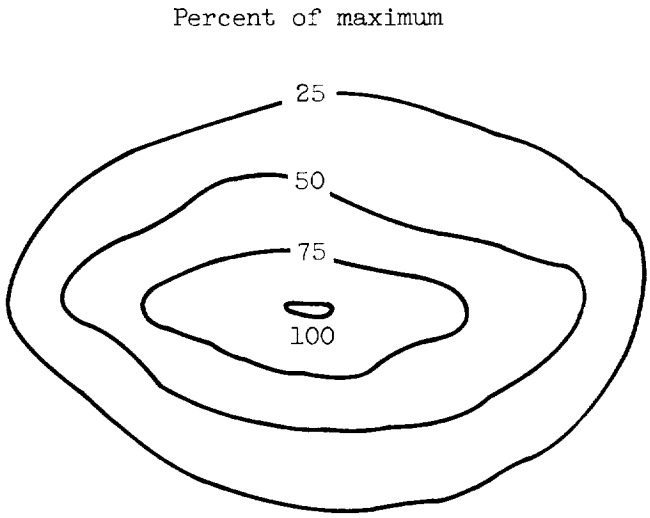

(a) Plate grid, 0.125-ampere beam at specific impulse of 5000 seconds.

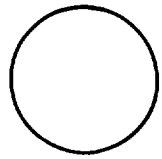

10-Cm-diam. source

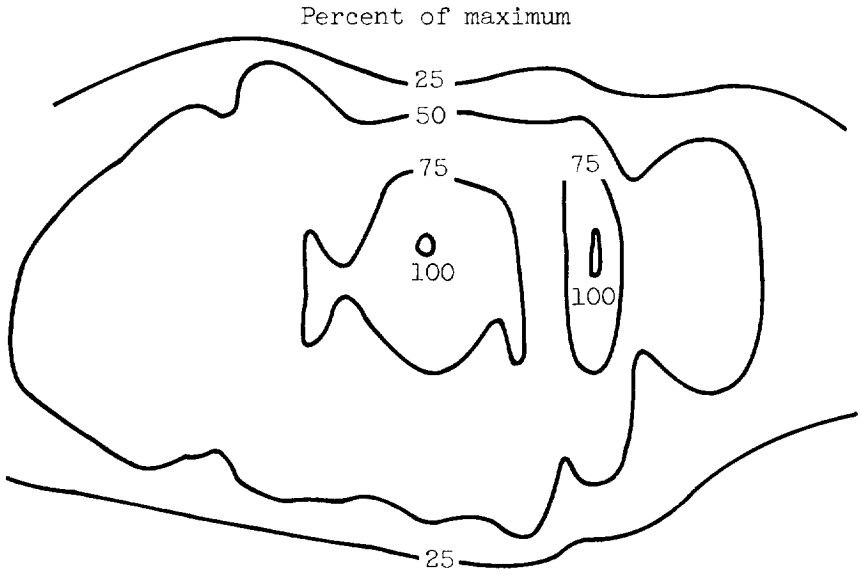

(b) Wire grid; 0.125-ampere beam at specific impulse of 6300 seconds.

Figure 12. - Comparison of beam power distribution for plate and wire accelerator systems. 1 Meter downstream of engine.

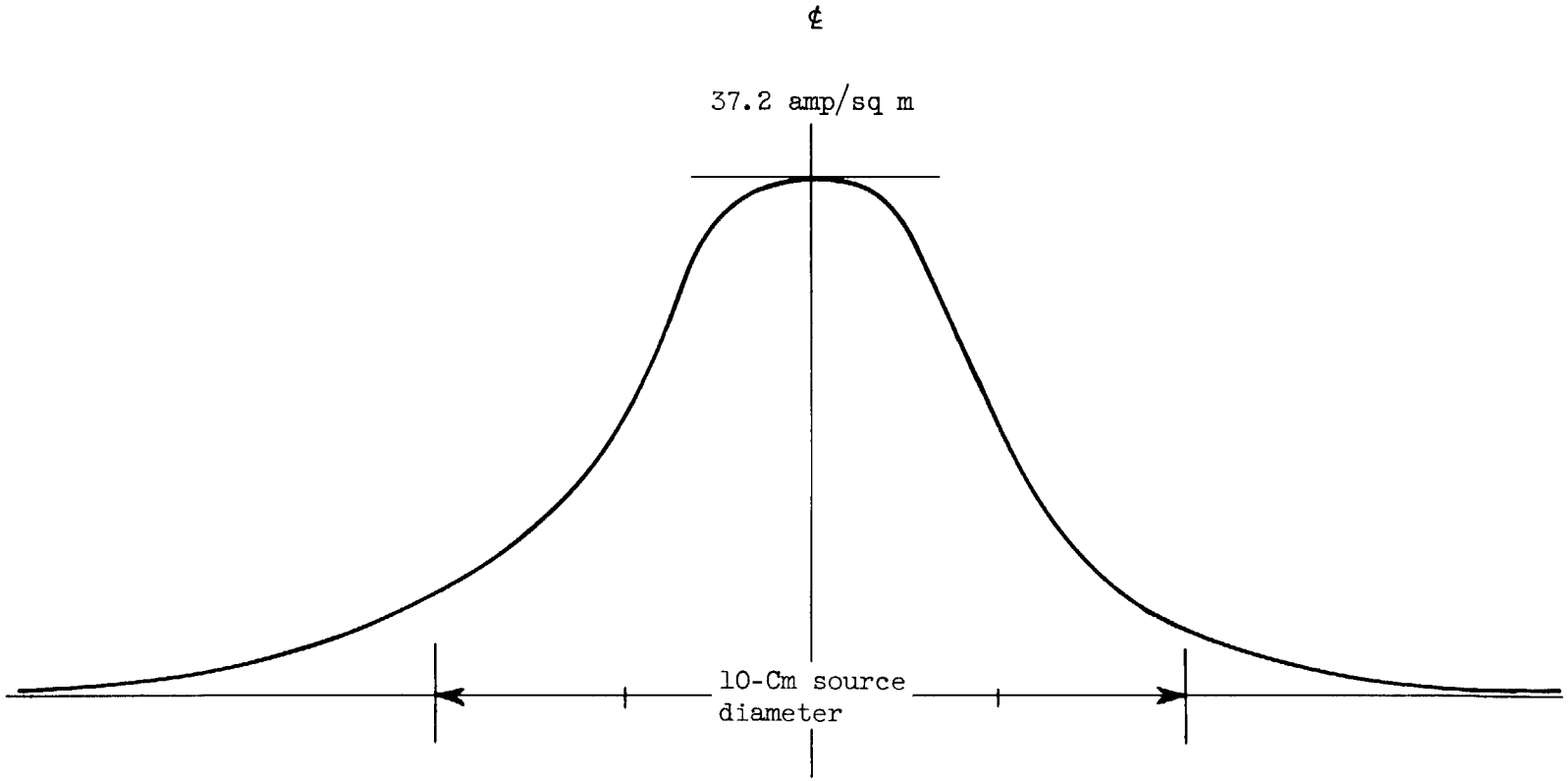

Figure 13. - Current distribution across downstream face of accelerator. 1/8-Ampere beam current at specific impulse of 6000 seconds.

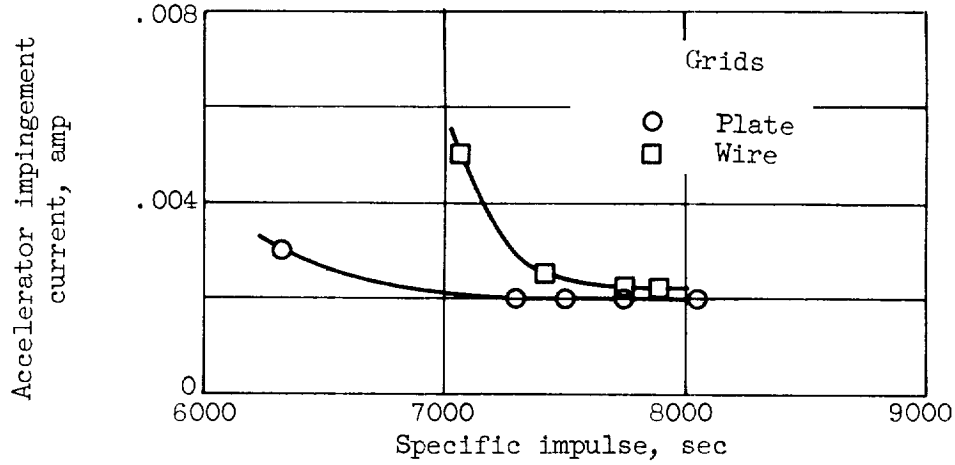

Figure 14. - Effect of specific impulse on accelerator impingement current at 0.25-ampere beam current. Propellant utilization efficiency, 80 percent.

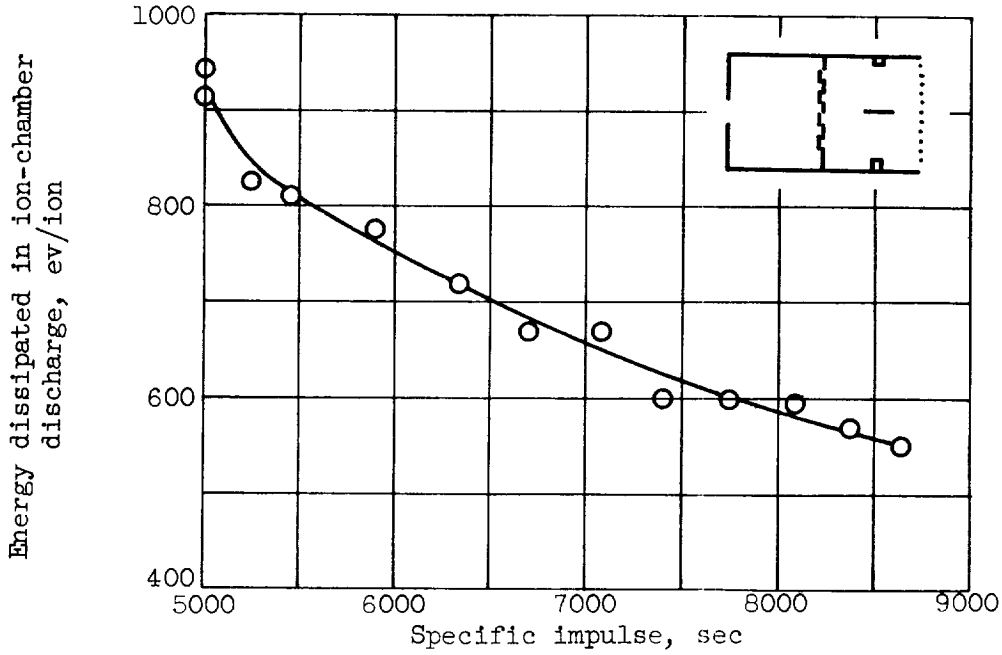

Figure 15. - Effect of specific impulse on ion-chamber efficiency with 0.125-ampere beam at propellant utilization efficiency of 80 percent. Nonuniform magnetic field; 1-centimeter anode in 10-centimeter-long ion chamber.

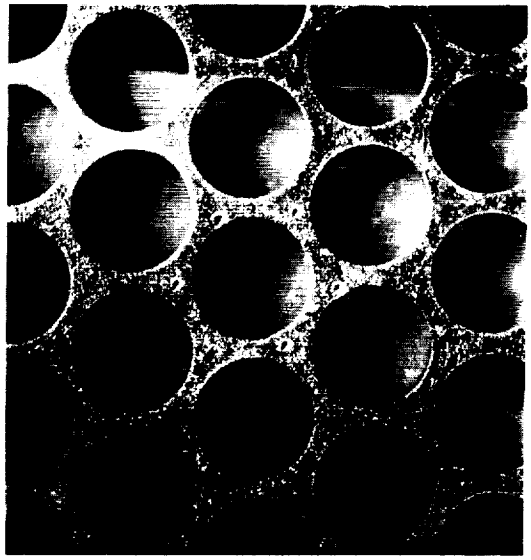

(a) General view of upstream face of accelerator grid after run.

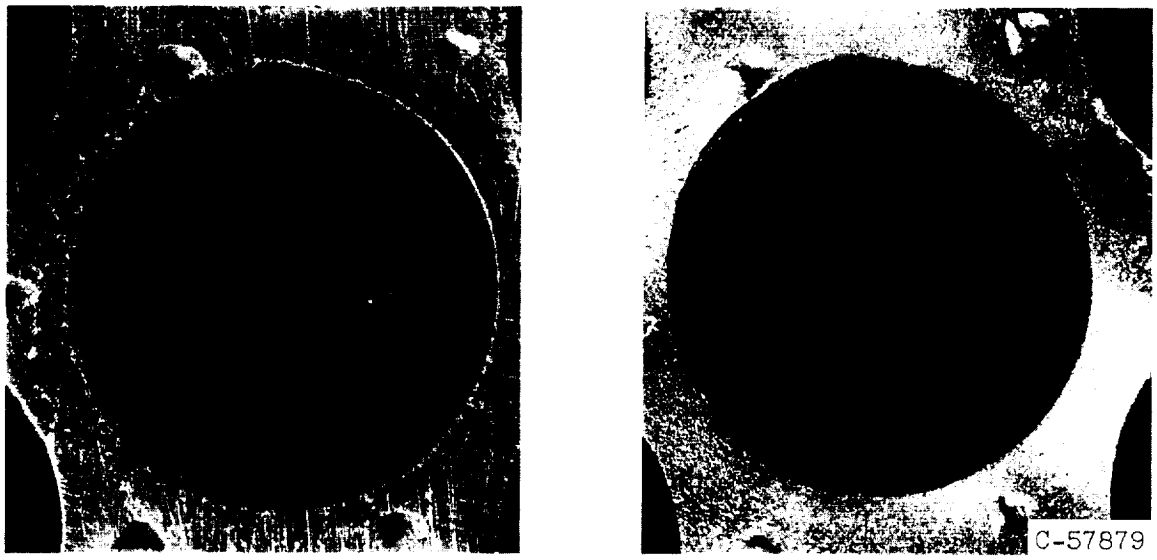

Before After

(b) Closeup of center hole.

Figure 16. - Impingement damage to molybdenum accelerator during 150-hour run with 0.2-ampere beam at specific impulse of 5000 seconds.

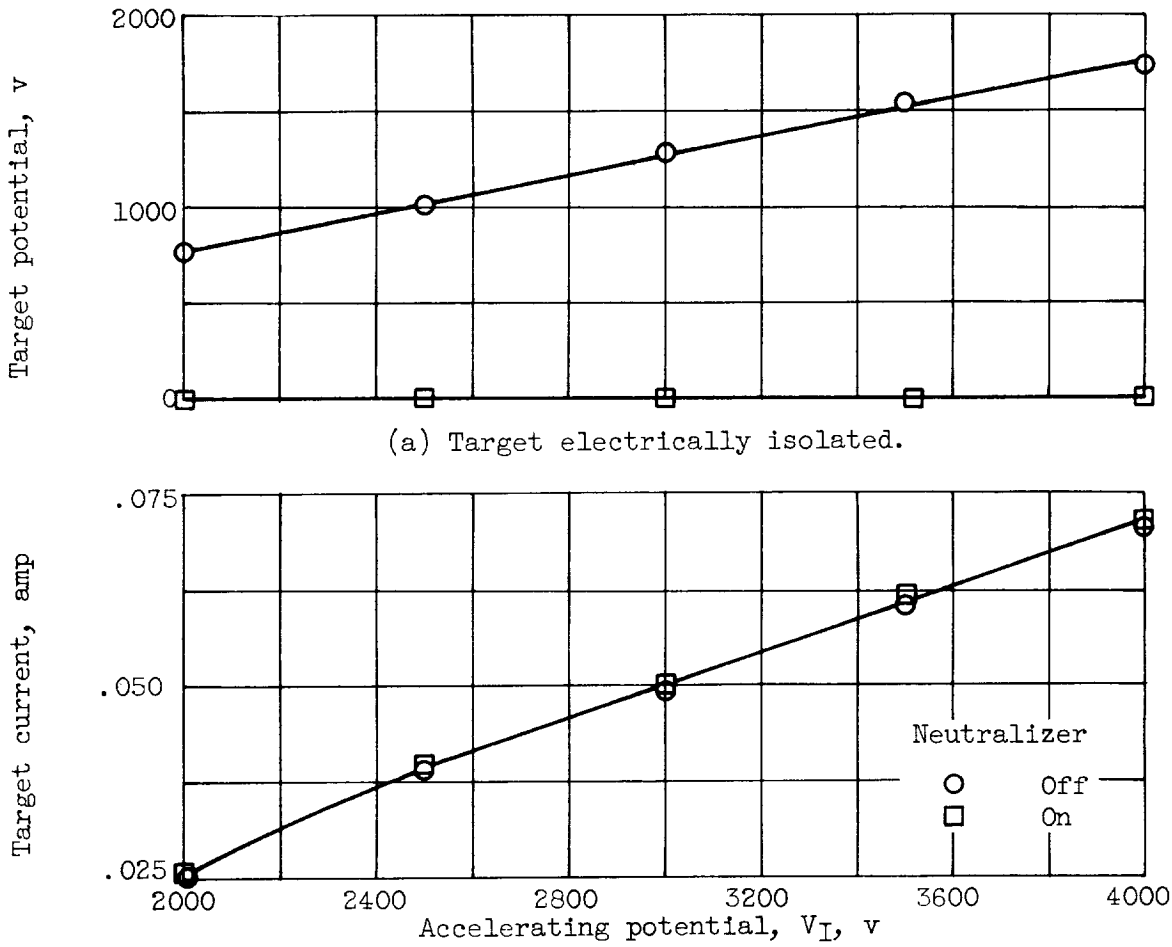

(a) Target electrically isolated.

(b) Target grounded through ammeter.

Figure 17. - Thrust target current and voltage as a function of net accelerating potential with and without neutralizer.